

Kerker Effects and Bound States in the Continuum in PT-Symmetric Dielectric Metasurfaces

Zhongqing Fang , Xiaofang Yang, Xiaolin Chen , Rugang Wang , Feng Zhou, Weibin Kong , and Chuanjie Chen

Abstract—We investigate the light transmission and reflection spectra of parity-time (PT) symmetric dielectric metasurfaces composed of high refractive index nanostructures with in-plane gain-loss modulation through the scattering matrix and semianalytical Cartesian multipoles methods. We find that the Kerker effects, i.e., the strong forward-to-backward asymmetric scattering originating from overlapping the electric and magnetic multipolar resonances, can be tailored by the gain and loss. In addition, we observe another kind of high-Q resonances, i.e., quasi-bound states in the continuum which couple to the electric and magnetic multipolar radiations, in the transmission and reflection spectra with different incident polarizations lights by manipulating the gain and loss in the metasurfaces. Our results suggest the ways to achieve Kerker effects and engineer the resonances in non-Hermitian metasurfaces for many practical applications in nanophotonics.

Index Terms—Kerker effects, bound states in the continuum, dielectric metasurfaces.

I. INTRODUCTION

METASURFACES, composed of two-dimensional arrangements of ultrathin subwavelength dielectric or metallic nanoparticles which supporting electric and magnetic multipole resonances and localized plasmonic resonances, have attracted a lot of interest in recent years due to the potential applications for manipulating the polarization, phase, amplitude and dispersion of light [1], [2]. Optical metasurfaces have been widely recognized for their capability to realize flat optical components and provide a playground for investigating the complex light-matter interactions at the nanoscale. A lot of novel optical

Manuscript received 14 June 2022; accepted 4 July 2022. Date of publication 7 July 2022; date of current version 18 July 2022. This work was supported in part by the National Natural Science Foundation of China under Grants 11801492, 62105087, and 61905059, in part by the Colleges and Universities Natural Science Foundation in Jiangsu Province under Grant 19KJA110002, in part by the Jiangsu Provincial Natural Science Foundation under Grant BK20181050, and in part by the Natural science research project of universities in Jiangsu Province under Grants 18KJD510010, 19KJB510061, 19KJB120014, and 20KJB140025. (Zhongqing Fang and Xiaofang Yang contributed equally to this work.) (Corresponding authors: Xiaolin Chen.)

Zhongqing Fang, Xiaofang Yang, Rugang Wang, Feng Zhou, Weibin Kong, and Chuanjie Chen are with the College of Information Engineering, Yancheng Institute of Technology, Yancheng 224051, China, and also with the Research Center of Photoelectric Technology, Yancheng Institute of Technology, Yancheng 224051, China (e-mail: fangzq@ycit.edu.cn; yangxf@ycit.cn; wrg3506@ycit.edu.cn; zhoulfeng@ycit.cn; kongweibin2007@sina.com; chencj@ycit.edu.cn).

Xiaolin Chen is with the Department of Optical Engineering, School of Physics, Hefei University of Technology, Hefei 230601, China (e-mail: chenxl-hfut@163.com).

Digital Object Identifier 10.1109/JPHOT.2022.3189025

properties have been theoretically and experimentally demonstrated, such as the photonic spin Hall effect [3], generalized laws of reflection and refraction [4], lattice resonances and lattice Kerker effects [5], generating broadband optical vortex beam [6] and bound states in the continuum (BICs) [7], [8]. A true BIC, including symmetry-protected and accidental BICs, is a nonradiating photonic eigenstate of wave equations embedded in the radiation continuum characterized by an infinite value of the Q factor and vanishing resonance width, i.e., they are discrete and spatially bounded, but exist at the same energy as a continuum of states which propagate to infinity. However, the symmetry-protected BIC can transform into quasi-BICs with high but finite Q factors controlled by symmetry-breaking perturbations [9]. What is more, BIC-inspired resonances are engineered for many important applications, such as polarization conversion [9].

Non-Hermitian physical systems, satisfying parity-time (PT) symmetry, have drawn great interest in recent decades due to the discovery of entire real spectra in complex Hamiltonians, which commute with the antilinear antiunitary PT operator, i.e., $[H, PT] = 0$, where the parity and time reversal operators amount to reversal of spatial ($\mathbf{r} \rightarrow -\mathbf{r}$) and time ($t \rightarrow -t$) coordinates, respectively [10]. The notion of PT-symmetry in non-Hermitian quantum mechanics can be extended to optics suggesting the complex refractive index profile of achiral medium with the form $n(\mathbf{r}) = n^*(-\mathbf{r})$, implying balanced loss and gain [11], [12]. In the context of optics and photonics, the gain and loss in materials can be integrated and controlled with high resolution with the advent of state-of-the-art fabrication methods and techniques, for example, the loss can arise from the ubiquitous materials absorption and radiation leakage to the external environment, and gain can be achieved through optical amplification with the aid of stimulated emission involving optical, electrical pumping or parametric processes [13]. So far a great deal of PT-symmetric optical systems have been theoretically and experimentally explored, such as two coupled optical resonators [14], coupled optical waveguides [13] and photonic waveguide lattices [15]. Accordingly, a wide range of intriguing counter-intuitive optical properties have been demonstrated, such as unidirectional invisibility [17], exceptional points (EPs) [13], [18], [19], loss induced optical transparency [20] and single mode laser [21].

Metasurfaces imbued with gain and loss provide an exciting venue to study the PT-symmetry [2], [22], such as PT symmetry breaking in polarization space [23], negative refraction

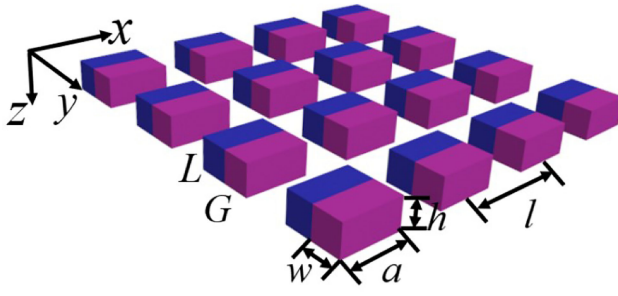


Fig. 1. Schematic illustration of the PT-symmetric metasurface illuminated by normal incident linearly polarized lights, the gain-loss modulation is along xy-plane with complex refractive index $n = 4 \pm i\kappa$ for loss medium (L) and gain medium (G), respectively. The subwavelength period of square lattice is designated as l , the side length and height of each nanoparticle are a and h , respectively. The width of loss and gain medium is w . The dielectric metasurface is suspended in vacuum.

and planar focusing [24], spectral singularities and asymmetric light scattering [25]. In this work, we study the optical properties of PT-symmetric dielectric metasurfaces composed of high refractive index nanostructures with the in-plane gain-loss modulation. By the application of scattering matrix and Cartesian multipoles methods, we find that the gain and loss can influence the Kerker effects, even achieving a broadband Kerker effect. In addition, a kind of high-Q resonances (quasi-BICs) which arising from a distortion of symmetry-protected BICs, can be excited by plane waves with different polarizations in the PT-symmetric metasurfaces. Our work shows that the gain and loss play an important role in optical properties of metasurfaces.

II. METHOD

The two-dimensional PT-symmetric metasurface composed of high refractive index nanoparticles (linear, nonmagnetic and isotropic materials) is shown in Fig. 1, the G and L represent gain and loss medium with complex refractive index $n = 4 - i\kappa$ and $n = 4 + i\kappa$, respectively. To investigate the transmission and reflection in the proposed reciprocal PT-symmetric metasurfaces, we use the scattering matrix (S-matrix which relates the incoming and outgoing waves or channels) defined as [26],

$$S = \begin{bmatrix} r_U & t \\ t & r_D \end{bmatrix}, \quad (1)$$

where the subscripts U/D denote the incident directions of plane waves along positive z axis and negative z axis, respectively. In our metasurface, the reflection amplitudes from the positive z axis and negative z axis are equal $r_U = r_D = r$. The transmission and reflection coefficients can be calculated through Cartesian multipole method [27]–[29]. According to the multipole representation (up to the second order) of the scattered electric field for a single nanoparticle,

$$\mathbf{E}^{sca}(\mathbf{n}) \sim [\mathbf{n} \times (\mathbf{p} \times \mathbf{n})] + \frac{1}{c} [\mathbf{m} \times \mathbf{n}] + \frac{ik}{6} [\mathbf{n} \times (\mathbf{n} \times \overset{\leftrightarrow}{Q}\mathbf{n})] + \frac{ik}{2c} [\mathbf{n} \times (\overset{\leftrightarrow}{M}\mathbf{n})], \quad (2)$$

where \mathbf{n} is the unit vector of the scattering direction, $k = \omega/c$ is the wave number in vacuum, \mathbf{p} and \mathbf{m} are the total electric

(ED) and magnetic dipole (MD) moments, $\overset{\leftrightarrow}{Q}$ and $\overset{\leftrightarrow}{M}$ are electric quadrupole (EQ) and magnetic quadrupole (MQ) moments, respectively. The definitions of Cartesian multipole moments are given at the appendix. The transmission and reflection amplitudes for x-polarized incident plane waves are,

$$r = \frac{ik}{E_{02}l^2\epsilon_0} \left(p_x - \frac{1}{c}m_y + \frac{ik}{6}Q_{xz} - \frac{ik}{2c}M_{yz} \right),$$

$$t = 1 + \frac{ik}{E_{02}l^2\epsilon_0} \left(p_x + \frac{1}{c}m_y - \frac{ik}{6}Q_{xz} - \frac{ik}{2c}M_{yz} \right), \quad (3)$$

where E_0 is the electric field of the normally incident plane waves at the center of nanoparticle, ϵ_0 is the vacuum permittivity and l^2 is the area of a lattice unit cell. In the case of y-polarized incident waves, we can rotate the metasurface to obtain the transmission and reflection amplitudes. The transmission and reflection coefficients are,

$$\mathbf{R} = |\mathbf{r}|^2, \mathbf{T} = |\mathbf{t}|^2. \quad (4)$$

The absorption coefficient can be derived through energy conservation, i.e., $A = 1 - T - R$. For PT-symmetric system, the transmission and reflection coefficients obey the generalized unitarity relation [30],

$$|\mathbf{T} - 1| = \mathbf{R}. \quad (5)$$

For $T < 1$, we can obtain the more familiar conservation relation $R + T = 1$ in optical system without gain and loss. After diagonalization, we can obtain the eigenvalues of scattering matrix,

$$s_n(\omega) = \mathbf{r} \pm \mathbf{t}. \quad (6)$$

It is worthy to note that there are no exception points (EPs) in the S-matrix of our metasurface [24]. When the angular frequency ω is analytically continued in the complex plane ($\omega = \omega_0 - i\gamma$), the eigenvalues can take any values between zero and infinity, which correspond to the zeros (perfect absorption) and poles (quasi-normal modes (QNMs)) of the S-matrix. A variety of scattering phenomena relate to the positions of poles and zeros of S-matrix, such as laser, CPA-laser and superscattering [31].

The finite element method (FEM) implemented in COMSOL Multiphysics was employed to calculate the optical response of the designed metasurfaces. The lattice period is fixed at $l = 350\text{nm}$ which is less than the whole range of interest wavelength suggesting that there no exist diffraction order of light. The side length, height and width of loss and gain medium of each nanoparticle are $a = 200\text{ nm}$, $h = 100\text{nm}$, $w = 100\text{nm}$, respectively. Bloch boundary conditions are applied to the unit cell, and the perfect matching layers (PMLs) are used to absorb reflected and transmitted light in the z directions. In addition, the port boundary conditions are also used to calculate the transmission, reflection and absorption spectra. Different mesh sizes inside and around the metasurface have been used in the simulations and the deviation of the results is found to be less than 1%, which indicates that the converged solutions are achieved.

III. RESULTS

We first consider the scattering properties of dielectric metasurface composed of high refractive index nanoparticles without

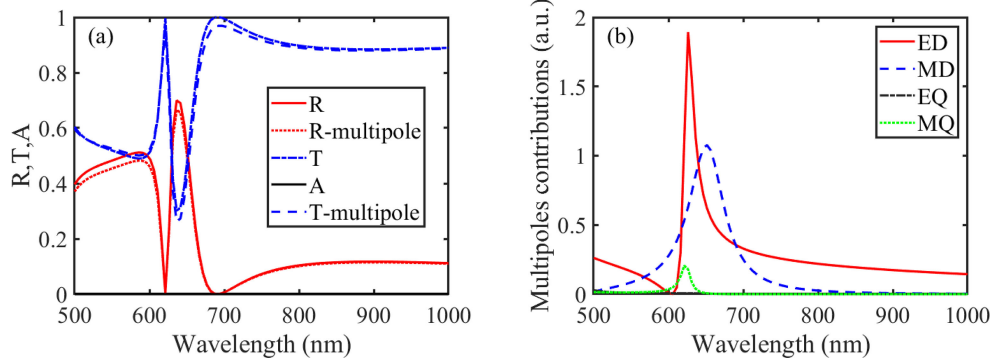


Fig. 2. (a) Spectra of transmission, reflection and absorption coefficients of the metasurface composed of high refractive index nanoparticles. The non-Hermitian parameter is $\kappa = 0$, and the lattice period is $l = 350$ nm. (b) The corresponding multipole decomposition contributions.

intrinsic loss and gain, i.e., $\kappa = 0$. The transmission, reflection and absorption spectra are shown in Fig. 2(a), which are calculated through full wave simulations and multipole decomposition method, respectively. We can see that the results of two methods are agreed very well. Fig. 2(b) shows the corresponding Mie multipolar contributions. The transmission, reflection and absorption spectra are the same for x-polarized and y-polarized incident plane waves as the square lattice belongs to D_{4h} point group. We can find that the light scattering properties of metasurfaces are mainly contributed by the electric dipole and magnetic dipole excited by incident plane wave, the contributions of electric quadrupole and magnetic quadrupole moments can be ignored, the overlapping electric and magnetic dipoles which are in-phase can satisfy the first Kerker's condition [32] $p = m/c$ at the wavelength $\lambda = 686$ nm and $\lambda = 621$ nm, the energies of light at these wavelengths are almost transmitted through the dielectric metasurface except for the changement of phase of light. When the incident wavelength is $\lambda = 636$ nm, the overlapping electric and magnetic dipoles are out-of-phase, and the second Kerker's condition [33] is satisfied $p = -m/c$, so the reflection coefficients approaches to unity. The overlapping electric and magnetic resonances can achieve a complete phase coverage from 0 to 2π for tailoring the wavefront of light [34].

Now we consider the transmission, reflection and absorption spectra of PT-symmetric metasurface, which are shown in Fig. 3(a). The polarization of incident plane wave is along x-direction, and the non-Hermitian parameter, i.e., gain-loss modulation, is $\kappa = 0.5$. The optical gain and loss in nanoparticles can be manipulated through p-type doping and quantum dots (Qdots) doping, such as PbS Qdots-doped glass through altering the Qdot diameter or the volume fraction [35], [36]. The calculated multipole contributions are shown in Fig. 3(b). From Fig. 3(c), we can see that the gain and loss play an import role in the Kerker's conditions, and the PT-symmetric metasurface can achieve a broadband unitary transmission with the wavelength varying from 621nm to 661nm due to the overlapping between electric and magnetic multipolar resonances, which are verified by the multipole decompositions as shown in Fig. 3(b). Fig. 3(c) depicts the evolution of transmission spectra of the metasurface composed of high refractive index nanoparticles with different non-Hermitian parameters, we can see that the broadband Kerker effect is strongly affected by the non-Hermitian parameters.

It is worthy to be noted that the absorption coefficient of PT-symmetric metasurface is vanishing, which is the same as the Hermitian metasurface without intrinsic gain and loss. This can be explained from the generalized conservation relation of PT-symmetric system, when the transmission coefficient is less than one, the relation $R + T = 1$ is satisfied, so the absorption coefficient is zero according to the conservation of energy, i.e., $R + T + A = 1$.

Apart from the electric and magnetic multipolar resonances in the transmission and reflection spectra, we can observe a sharp Fano resonance at the wavelength $\lambda = 803$ nm, i.e., quasi-BIC. From Fig. 3(b), we can conclude that the Fano resonance results from the profile of electric multipolar resonance. Ignoring the other multipolar contributions, the transmission and reflection amplitudes are,

$$\begin{aligned} r &= \frac{ik}{E_{02}l^2\epsilon_0} p_x, \\ t &= 1 + \frac{ik}{E_{02}l^2\epsilon_0} p_x, \end{aligned} \quad (7)$$

The eigenvalues of scattering matrix are,

$$s_n(\omega) = 1 + \frac{ik}{E_0 l^2 \epsilon_0} p_x, -1. \quad (8)$$

From the Eqs. (7) and (8), the poles of S-matrix are the same as the reflection amplitudes, one eigenvalue can exhibit a sharp peak, while one eigenvalue becomes a constant, the BIC can be achieved through moving the poles and scattering zeros (called reflectionless scattering modes) of S-matrix closer to each other until they get coalesced at the real frequencies [31].

To further demonstrate the sharp Fano resonance resulting from the BICs, we perform an eigenfrequency analysis and calculate the quality factors (Q) of resonant eigenmodes using COMSOL, which are shown in Fig. 3(d). we can see that the quality factor is extremely high when the non-Hermitian parameter is $\kappa = 0$, the bound states in the continuum becomes leaky resonance which couples to the electric multipolar radiations with increasing the non-Hermitian parameter. The quality factor is $Q = 768$ when the non-Hermitian parameter is $\kappa = 0.5$. The electric field intensity distribution of high-Q mode regarded as TE mode with $E_z = 0$ in the x-y plane and the x-z plane, is shown in Fig. 3(e) and 3(f), respectively. we can see that it slightly lost the in-plane symmetry which also demonstrate the leaky feature of high-Q resonance.

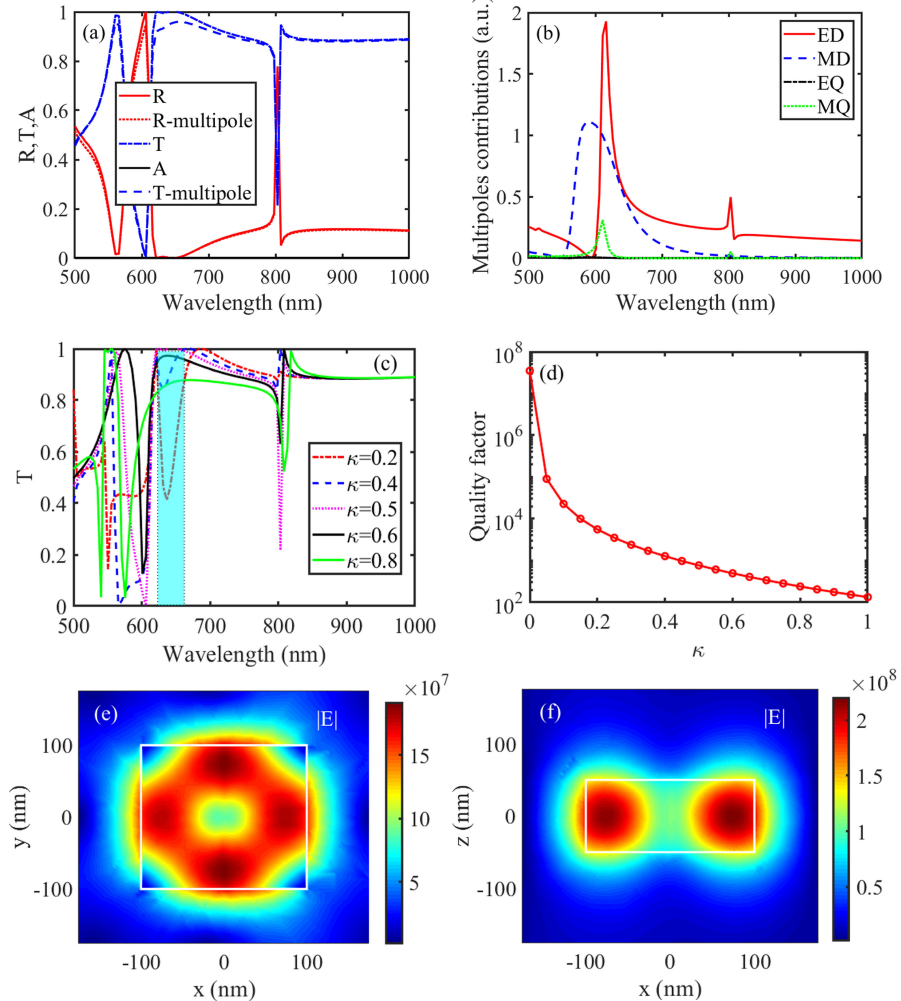


Fig. 3. (a) Spectra of transmission, reflection and absorption coefficients of PT-symmetric metasurface composed of high refractive index nanoparticles illuminated by normally incident x-polarized light. The non-Hermitian parameter is $\kappa = 0.5$, and the lattice period is $l = 350$ nm. (b) The corresponding multipole decomposition contributions. (c) The transmission spectra of the metasurface composed of high refractive index nanoparticles with different non-Hermitian parameters ($\kappa = 0.2, 0.4, 0.5, 0.6$ and 0.8). (d) The quality factors of high-Q modes as a function of non-Hermitian parameters. The electric field intensity distribution of TE high-Q mode with $\kappa = 0.5$ in the x-y plane (e) and x-z plane (f).

In the case of normally incident y-polarized light, the transmission, reflection and absorption spectra of PT-symmetric metasurface are shown in Fig. 4(a). The non-Hermitian parameter is also fixed at $\kappa = 0.5$, and the lattice period is $l = 350$ nm. The corresponding multipole decomposition contributions are shown in Fig. 4(b). From Fig. 4(a), we also observe the first Kerker's condition when the incident wavelengths are at $\lambda = 611$ nm and $\lambda = 671$ nm, respectively. In addition, there also exist sharp Fano resonances in the transmission and reflection coefficients at the wavelength $\lambda = 505$ nm and $\lambda = 560$ nm. Especially, we pay attention to the sharp Fano resonance at the wavelength $\lambda = 560$ nm. As seen from Fig. 4(b), the sharp Fano resonance results from the profile of magnetic multipolar resonances, one of eigenvalues of scattering matrix is approximately $s_n(\omega) \propto m_y$, which demonstrates the emergence of pole of S-matrix. We also calculate the quality factors of high-Q mode regarded as TM mode with $H_z = 0$ as a function of gain and loss modulation, as shown in Fig. 4(c). When the non-Hermitian parameter is $\kappa = 0.5$, the quality factor is $Q = 349$ and the quasi-BIC couples to the magnetic multipolar

radiations, the corresponding slightly asymmetric magnetic field intensity distributions in the x-y plane and the x-z plane are shown in Fig. 4(d) and 4(e), respectively. They also demonstrate the high-Q resonance governed by quasi-BIC.

The BICs exhibits a topological nature associated with vortex centers in the polarization directions of far-field radiation, i.e., polarization singularity, which carries the quantized topological charges defined as [7], [37], [38],

$$\mathbf{q} = \frac{1}{2\pi} \oint d\mathbf{k} \cdot \nabla_{\mathbf{k}} \varphi(\mathbf{k}), \quad (9)$$

where the $\varphi(\mathbf{k})$ is the angle of polarization vector and the integration is taken a closed path in k -space that goes around the BICs in the counterclockwise direction. The polarization vector transforms back to itself after a closed loop with an integer multiple of 2π (winding number) for the overall angle of polarization vector. We choose a circle with $|\mathbf{k}| = 0.05\pi/l$ as an integration path and set the non-Hermitian parameter $\kappa = 0$, finally we obtain the topological charges for TE and TM modes with $q = 1$. To further investigate the topology of

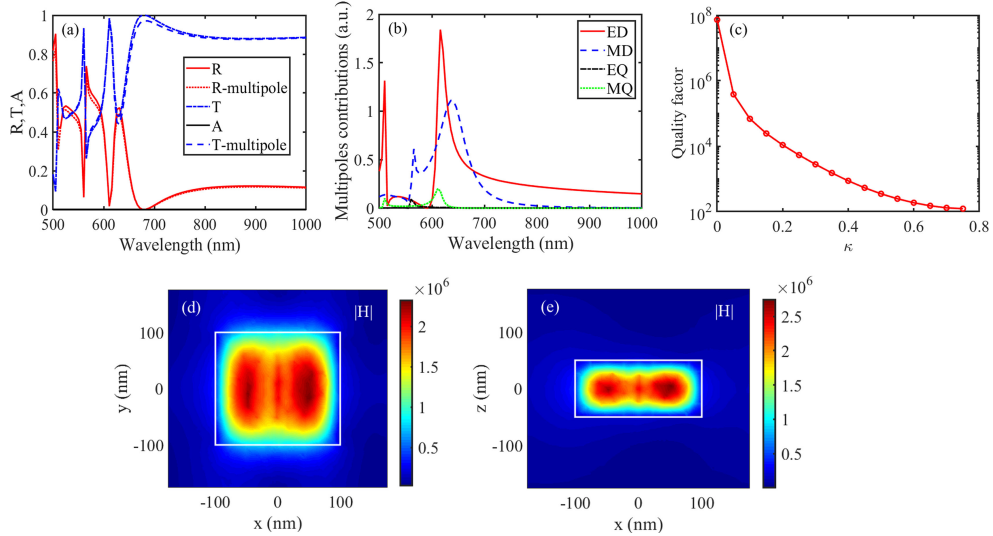


Fig. 4. (a) Spectra of transmission, reflection and absorption coefficients of PT-symmetric metasurface composed of high refractive index nanoparticles which is illuminated by normally incident y-polarized light. The non-Hermitian parameter is $\kappa = 0.5$, and the lattice period is $l = 350$ nm. (b) The corresponding multipole decomposition contributions. (c) The quality factor of high-Q mode as a function of non-Hermitian parameter. (d) The magnetic field intensity distribution of TM high-Q mode with $\kappa = 0.5$ in the x-y plane. (e) The magnetic field intensity distribution of TM high-Q mode with $\kappa = 0.5$ in the x-z plane.

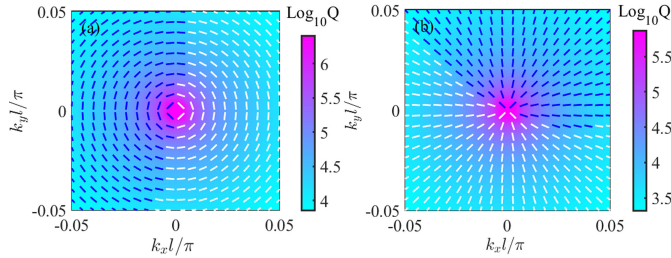


Fig. 5. (a) Far-field polarization states and quality factors distribution of TE BIC with $\kappa = 0$. (b) Far-field polarization states and quality factor distributions of TM BIC with $\kappa = 0$.

polarization singularity in k -space, we can project the far-fields of Bloch mode, of which the electric field E_x and E_y are spatially averaged over one unit cell on any horizontal plane outside the metasurface, onto x-y plane and introduce the normalized Stokes parameters,

$$\begin{aligned} S_1 &= \frac{|E_x(\mathbf{k})|^2 - |E_y(\mathbf{k})|^2}{|E_x(\mathbf{k})|^2 + |E_y(\mathbf{k})|^2}, \\ S_2 &= \frac{2\text{Re}[E_x E_y^*]}{|E_x(\mathbf{k})|^2 + |E_y(\mathbf{k})|^2}, \\ S_3 &= \frac{-2\text{Im}[E_x E_y^*]}{|E_x(\mathbf{k})|^2 + |E_y(\mathbf{k})|^2}, \end{aligned} \quad (10)$$

where $\varphi(\mathbf{k}) = 1/2\arg[S_1(\mathbf{k}) + iS_2(\mathbf{k})]$ and V points represent BICs with $S_1 = S_2 = S_3 = 0$. The far-field polarization and quality factor distributions of TE and TM BICs are shown in Fig. 5. It can be seen from Fig. 5a and 5b that the quality factor of TE and TM modes with $\mathbf{k} = 0$ is very large. The polarization vortexes also indicate that the TE and TM BICs carry a topological charge with $q = 1$.

IV. CONCLUSION

We have studied the transmission, reflection and absorption properties of PT-symmetric metasurfaces composed of high refractive index nanoparticles, we find that Kerker effects, even a broadband Kerker effect, originating from overlapping the electric and magnetic multipolar resonances can be achieved in non-Hermitian photonic system through adjusting the gain and loss. The absorption coefficient of PT-symmetric metasurfaces is vanishing. In addition, there exist sharp Fano resonances, i.e., quasi-BICs, in the transmission and reflection spectra which are different from the electric and magnetic multipolar resonances. The calculated topological charges of BICs are 1. Our work will pave the way for studying the Kerker effect and BICs in PT-symmetric systems and suggesting the practical applications for optical trapping, biological sensing and quantum information.

Declaration of Competing Interest: The authors declare that they have no known competing financial interests or personal relationships that could have appeared to influence the work reported in this paper.

Cartesian Multipole Moments: The multipole moments in the Cartesian representations for electric dipole, magnetic dipole, electric quadrupole and magnetic quadrupole, respectively, are given as,

$$\begin{aligned} \mathbf{P} &= \int \mathbf{P} j_0(kr) dr + \frac{k^2}{10} \int \left\{ [\mathbf{r} \cdot \mathbf{P}] \mathbf{r} - \frac{1}{3} r^2 \mathbf{P} \right\} \frac{15j_2(kr)}{(kr)^2} dr, \\ \mathbf{m} &= -\frac{i\omega}{2} \int [\mathbf{r} \times \mathbf{P}] \frac{3j_1(kr)}{kr} dr, \\ \overset{\leftrightarrow}{Q} &= \int \left\{ 3(\mathbf{r} \otimes \mathbf{P} + \mathbf{P} \otimes \mathbf{r}) - 2[\mathbf{r} \cdot \mathbf{P}] \overset{\leftrightarrow}{I} \right\} \frac{3j_1(kr)}{kr} dr \\ &\quad + 6k^2 \times \int \left\{ 5\mathbf{r} \otimes \mathbf{r} [\mathbf{r} \cdot \mathbf{P}] - (\mathbf{r} \otimes \mathbf{P} \right. \\ &\quad \left. + \mathbf{P} \otimes \mathbf{r}) r^2 - r^2 [\mathbf{r} \cdot \mathbf{P}] \overset{\leftrightarrow}{I} \right\} \frac{j_3(kr)}{(kr)^3} dr, \end{aligned}$$

$$\overset{\leftrightarrow}{M} = \frac{\omega}{3i} \int \{[\mathbf{r} \times \mathbf{P}] \otimes \mathbf{r} + \mathbf{r} \otimes [\mathbf{r} \times \mathbf{P}]\} \frac{15j_2(kr)}{(kr)^2} d\mathbf{r},$$

where j_n is the n -order spherical Bessel function, $\mathbf{P} = \epsilon_0(\epsilon - 1)\mathbf{E}(\mathbf{r})$ is the light-induced polarization with the relative dielectric permittivity ϵ and total electric field $\mathbf{E}(\mathbf{r})$ inside the nanoparticles. The time factor is $e^{-i\omega t}$.

REFERENCES

- [1] P. Genevet, F. Capasso, F. Aieta, M. Khorasaninejad, and R. Devlin, "Recent advances in planar optics: From plasmonic to dielectric metasurfaces," *Optica*, vol. 4, no. 1, pp. 139–152, Jan. 2017, doi: [10.1364/OPTICA.4.000139](#).
- [2] A. Vaskin, R. Kolkowski, A. F. Koenderink, and I. Staude, "Light-emitting metasurfaces," *Nanophotonics*, vol. 8, no. 7, pp. 1151–1198, Jun. 2019, doi: [10.1515/nanoph-2019-0110](#).
- [3] X. Yin, Z. Ye, J. Rho, Y. Wang, and X. Zhang, "Photonic spin hall effect at metasurfaces," *Science*, vol. 339, no. 6126, pp. 1405–1407, Mar. 2013, doi: [10.1126/science.1231758](#).
- [4] N. Yu *et al.*, "Light propagation with phase discontinuities: Generalized laws of reflection and refraction," *Science*, vol. 334, no. 6054, pp. 333–337, Sep. 2011, doi: [10.1126/science.1210713](#).
- [5] V. E. Babicheva and A. B. Evlyukhin, "Resonant lattice kerker effect in metasurfaces with electric and magnetic optical responses," *Laser Photon. Rev.*, vol. 11, no. 6, Oct. 2017, Art. no. 1700132, doi: [10.1002/lpor.201700132](#).
- [6] L. Huang *et al.*, "Dispersionless phase discontinuities for controlling light propagation," *Nano Lett.*, vol. 12, no. 11, pp. 5750–5755, Oct. 2012, doi: [10.1021/nl303031j](#).
- [7] K. Koshelev, S. Lepeshov, M. Liu, A. Bogdanov, and Y. Kivshar, "Asymmetric metasurfaces with high-Q resonances governed by bound states in the continuum," *Phys. Rev. Lett.*, vol. 121, no. 19, Nov. 2018, Art. no. 193903, doi: [10.1103/PhysRevLett.121.193903](#).
- [8] Q. Song, S. Dai, D. Z. Han, Z. Q. Zhang, and J. Zi, "PT symmetry induced rings of lasing threshold modes embedded with discrete bound states in the continuum," *Chin. Phys. Lett.*, vol. 38, no. 8, Aug. 2021, Art. no. 84203, doi: [10.1088/0256-307X/38/8/084203](#).
- [9] X. Chen, Y. Zhou, X. Ma, W. Fang, W. Zhang, and W. Gao, "Polarization conversion in anisotropic dielectric metasurfaces originating from bound states in the continuum," *Opt. Lett.*, vol. 46, no. 17, pp. 4120–4123, Aug. 2021, doi: [10.1364/OL.431047](#).
- [10] C. M. Bender and S. Boettcher, "Real spectra in nonhermitian Hamiltonians having PT symmetry," *Phys. Rev. Lett.*, vol. 80, no. 24, pp. 5243–5246, Jun. 1998, doi: [10.1103/PhysRevLett.80.5243](#).
- [11] A. A. Zyablovsky, A. P. Vinogradov, A. A. Pukhov, A. V. Dorofeenko, and A. A. Lisyansky, "PT-symmetry in optics," *Phys.-Uspekhi*, vol. 57, no. 11, pp. 1063–1082, Apr. 2014, doi: [10.3367/UFN.0184.201411b.1177](#).
- [12] S. Droulias, I. Katsantonis, M. Kafesaki, C. M. Soukoulis, and E. N. Economou, "Chiral metamaterials with pt symmetry and beyond," *Phys. Rev. Lett.*, vol. 122, no. 21, May 2019, Art. no. 213201, doi: [10.1103/PhysRevLett.122.213201](#).
- [13] M. A. Miri and A. Alù, "Exceptional points in optics and photonics," *Science*, vol. 363, no. 6422, Jan. 2019, Art. no. 7709, doi: [10.1126/science.aar7709](#).
- [14] B. Peng *et al.*, "Parity-time-symmetric whispering-gallery microcavities," *Nature Phys.*, vol. 10, no. 5, pp. 394–398, Apr. 2014, doi: [10.1038/nphys2927](#).
- [15] S. Klaiman, U. Günther, and N. Moiseyev, "Visualization of branch points in PT-symmetric waveguides," *Phys. Rev. Lett.*, vol. 101, no. 8, Aug. 2008, Art. no. 080402, doi: [10.1103/PhysRevLett.101.080402](#).
- [16] M. Kremer, T. Biesenthal, L. J. Maczewsky, M. Heinrich, R. Thomale, and A. Szameit, "Demonstration of a two-dimensional PT-symmetric crystal," *Nature Commun.*, vol. 10, no. 1, pp. 1–7, Jan. 2019, doi: [10.1038/s41467-018-08104-x](#).
- [17] Z. Lin, H. Ramezani, T. Eichelkraut, T. Kottos, H. Cao, and D. N. Christodoulides, "Unidirectional invisibility induced by PT-symmetric periodic structures," *Phys. Rev. Lett.*, vol. 106, no. 21, May 2011, Art. no. 213901, doi: [10.1103/PhysRevLett.106.213901](#).
- [18] M. Sakhdari, M. Hajizadegan, Q. Zhong, D. Christodoulides, R. El-Ganainy, and P.-Y. Chen, "Experimental observation of PT symmetry breaking near divergent exceptional points," *Phys. Rev. Lett.*, vol. 123, no. 19, Nov. 2019, Art. no. 193901, doi: [10.1103/PhysRevLett.123.193901](#).
- [19] X. Chen, H. Wang, J. Li, K. Wong, and D. Lei, "Scattering asymmetry and circular dichroism in coupled PT-symmetric chiral nanoparticles," *Nanophotonics*, vol. 11, no. 9, pp. 2159–2167, May 2022, doi: [10.1515/nanoph-2021-0705](#).
- [20] A. Guo *et al.*, "Observation of PT-symmetry breaking in complex optical potentials," *Phys. Rev. Lett.*, vol. 103, no. 9, Aug. 2009, Art. no. 093902, doi: [10.1103/PhysRevLett.103.093902](#).
- [21] L. Feng, Z. J. Wong, R.-M. Ma, Y. Wang, and X. Zhang, "Single-mode laser by parity-time symmetry breaking," *Science*, vol. 346, no. 6212, pp. 972–975, Nov. 2014, doi: [10.1126/science.1258479](#).
- [22] V. C. Su, C. H. Chu, G. Sun, and D. P. Tsai, "Advances in optical metasurfaces: Fabrication and applications," *Opt. Exp.*, vol. 26, no. 10, pp. 13148–13182, May 2018, doi: [10.1364/OE.26.013148](#).
- [23] M. Lawrence *et al.*, "Manifestation of PT symmetry breaking in polarization space with terahertz metasurfaces," *Phys. Rev. Lett.*, vol. 113, no. 9, Aug. 2014, Art. no. 093901, doi: [10.1103/PhysRevLett.113.093901](#).
- [24] R. Fleury, D. L. Sounas, and A. Alù, "Negative refraction and planar focusing based on parity-time symmetric metasurfaces," *Phys. Rev. Lett.*, vol. 113, no. 2, Aug. 2014, Art. no. 023903, doi: [10.1103/PhysRevLett.113.023903](#).
- [25] J. Tapar, S. Kishen, and N. K. Emani, "Spectral singularities and asymmetric light scattering in PT-symmetric 2D nanoantenna arrays," *Opt. Lett.*, vol. 45, no. 18, pp. 5185–5188, Sep. 2020, doi: [10.1364/OL.398551](#).
- [26] Y. Chong, L. Ge, and A. D. Stone, "Pt-symmetry breaking and laser-absorber modes in optical scattering systems," *Phys. Rev. Lett.*, vol. 108, no. 26, Mar. 2011, Art. no. 093902, doi: [10.1103/PhysRevLett.106.093902](#).
- [27] P. D. Terekhov, V. E. Babicheva, K. V. Baryshnikova, A. S. Shalin, A. Karabchevsky, and A. B. Evlyukhin, "Multipole analysis of dielectric metasurfaces composed of nonspherical nanoparticles and lattice invisibility effect," *Phys. Rev. B*, vol. 99, no. 4, Jan. 2019, Art. no. 045424, doi: [10.1103/PhysRevB.99.045424](#).
- [28] A. B. Evlyukhin, C. Reinhardt, A. Seidel, B. S. Lukyanchuk, and B. N. Chichkov, "Optical response features of si-nanoparticle arrays," *Phys. Rev. B*, vol. 82, no. 4, Jan. 2019, Art. no. 045404, doi: [10.1103/PhysRevB.82.045404](#).
- [29] X. Chen *et al.*, "Magnetic purcell effect in all-dielectric periodic optical antennas," *Opt. Commun.*, vol. 519, no. 15, Sep. 2022, Art. no. 128427, doi: [10.1016/j.optcom.2022.128427](#).
- [30] L. Ge, Y. Chong, and A. D. Stone, "Conservation relations and anisotropic transmission resonances in one-dimensional PT-symmetric photonic heterostructures," *Phys. Rev. A*, vol. 85, no. 4, Feb. 2012, Art. no. 023802, doi: [10.1103/PhysRevA.85.023802](#).
- [31] A. Krasnok, D. Baranov, H. Li, M.-A. Miri, F. Monticone, and A. Alù, "Anomalies in light scattering," *Adv. Opt. Photon.*, vol. 11, no. 4, pp. 892–951, Dec. 2019, doi: [10.1364/AOP.11.000892](#).
- [32] M. F. Picardi, A. V. Zayats, and F. J. Rodriguez-Fortuno, "Janus and huygens dipoles: Near-field directionality beyond spin-momentum locking," *Phys. Rev. Lett.*, vol. 120, no. 11, Mar. 2018, Art. no. 117402, doi: [10.1103/PhysRevLett.120.117402](#).
- [33] J. Olmos-Trigo *et al.*, "Kerker conditions upon lossless, absorption, and optical gain regimes," *Phys. Rev. Lett.*, vol. 125, no. 7, Aug. 2020, Art. no. 073205, doi: [10.1103/PhysRevLett.125.073205](#).
- [34] M. Decker *et al.*, "High efficiency dielectric huygens surfaces," *Adv. Opt. Mater.*, vol. 3, no. 6, pp. 813–820, Feb. 2015, doi: [10.1002/adom.201400584](#).
- [35] Y. M. Xie, W. Tan, and Z. G. Wang, "Anomalous forward scattering of dielectric gain nanoparticles," *Opt. Exp.*, vol. 23, no. 3, pp. 2091–2100, Feb. 2015, doi: [10.1364/OE.23.002091](#).
- [36] J. Tapar, S. Kishen, K. Prashant, K. Nayak, and N. K. Emani, "Enhancement of the optical gain in GaAs nanocylinders for nanophotonic applications," *J. Appl. Phys.*, vol. 127, no. 15, Apr. 2020, Art. no. 153102, doi: [10.1063/1.5132613](#).
- [37] B. Zhen, C. W. Hsu, L. Lu, A. D. Stone, and M. Soljacic, "Topological nature of optical bound states in the continuum," *Phys. Rev. Lett.*, vol. 113, no. 25, Dec. 2014, Art. no. 257401, doi: [10.1103/PhysRevLett.113.257401](#).
- [38] Y. Zeng, G. Hu, K. Liu, Z. Tang, and C. W. Qiu, "Dynamics of topological polarization singularity in momentum space," *Phys. Rev. Lett.*, vol. 127, no. 17, Sep. 2021, Art. no. 176101, doi: [10.1103/PhysRevLett.127.176101](#).